

Valence bond crystal and possible orbital pinball liquid in a t_{2g} model

Fabien Trouselet

Max-Planck-Institut für Festkörperforschung, Heisenbergstrasse 1, D-70569 Stuttgart, Germany

Arnaud Ralko

Institut Néel, UPR2940, CNRS et Université de Grenoble, Grenoble, F-38042 France

Andrzej M. Oleś

Max-Planck-Institut für Festkörperforschung, Heisenbergstrasse 1, D-70569 Stuttgart, Germany and Marian Smoluchowski Institute of Physics, Jagellonian University, Reymonta 4, PL-30059 Kraków, Poland

(Dated: November 10, 2018)

We study a model for orbitally degenerate Mott insulators, where localized electrons possess t_{2g} degrees of freedom coupled by several, competing, exchange mechanisms. We provide evidence for two distinct strongly fluctuating regimes, depending on whether superexchange or direct exchange mechanism predominates. In the superexchange-dominated regime, the ground state is dimerized, with nearest neighbor orbital singlets covering the lattice. By deriving an effective quantum dimer model and analyzing it numerically, we characterize this dimerized phase as a valence bond crystal stabilized by singlet resonances within a large unit cell. In the opposite regime, with predominant direct exchange, the combined analysis of the original model and another effective model adapted to the local constraints shows that subleading perturbations select a highly resonating ground state, with coexisting diagonal and off-diagonal long-range orbital orders.

Published in: Phys. Rev. B **86**, 014432 (2012).

PACS numbers: 75.10.Kt, 03.65.Ud, 64.70.Tg, 75.10.Jm

I. INTRODUCTION

One of the most intriguing concepts in contemporary condensed matter physics is the possibility to stabilize phases without any broken symmetry at low temperature. In strongly correlated materials, e.g. in transition metal oxides, charge degrees of freedom are localized due to large Coulomb interactions and both spin and orbital degrees of freedom interact with each other and may remain disordered. While numerous realizations of quantum spin liquids, such as resonating valence bond (RVB) phases, have been reported both experimentally and theoretically,¹ there are only few examples of orbital liquids in Mott insulators up to now.²⁻⁴ Usually orbitals are accompanied by spins and frustrated interactions in both subsystems could imply a spin-orbital liquid phase. If spin and orbital variables are coupled to each other by relativistic effects, such a phase may emerge from effective pseudospin interactions on a honeycomb lattice.⁵ For the superexchange interactions in transition metal oxides,⁶ a spin-orbital liquid could be stabilized in presence of geometrical frustration.⁷ For instance, it was suggested as the ground state on a triangular lattice for LiNiO_2 with active e_g orbitals.⁸ It would explain the absence of symmetry breaking with spin and orbital order, but the realistic situation in this compound is more subtle.⁹ However, it was shown recently that the paradigm of a spin-orbital liquid can be realized on the triangular lattice in a system with active t_{2g} orbitals,¹⁰⁻¹² given by the (111)-plane of Ti^{3+} ions in NaTiO_2 .

The spin-orbital systems are rather complex and difficult to analyze as spin and orbital operators are frequently highly entangled¹³ and it is not trivial to recognize which part of the interactions is most frustrated. Therefore, considering simpler and easier tractable models with only orbital variables

(and frozen spins) became recently fashionable as, in this way, the intrinsically frustrated orbital interactions could be directly investigated. These interactions have only the lattice symmetries,² in contrast to high $\text{SU}(2)$ symmetry of spin interactions. For a two-dimensional (2D) e_g orbital model one finds competing yet robust orbital ordered phases.¹⁴ In fact, in this case frustration is not yet maximal and increases further when the interactions are modified and the 2D compass model limit is approached.¹⁵ In this limit the system is still in the 2D Ising universality class¹⁶ and orbital order persists in a range of finite temperature.¹⁷

Three-dimensional (3D) orbital models are characterized by an even stronger frustration but an order by disorder mechanism stabilizes an ordered phase in the e_g orbital model,¹⁸ as shown recently by Monte Carlo simulations.¹⁹ The situation in the 3D compass limit, also referred to as the classical t_{2g} model, is still controversial: while the absence of a phase transition at finite temperature was conjectured by a high-temperature series expansion,²⁰ a first order transition into a low-temperature lattice-nematic phase without any orbital order was found by Monte Carlo simulations.²¹

Geometrically frustrated t_{2g} orbital systems on the triangular lattice have been studied recently by effective models for large Coulomb interactions.¹⁰⁻¹² These studies led to identification of a variety of exotic ground states, depending on the parameters governing electron hoppings and interactions. Several of them were characterized by dimerization into either spin- or orbital-singlet phases — this enables a description by an effective quantum dimer model (QDM),^{8,12,22} and opens a route towards the possibility of a spin-orbital liquid¹¹ in a regime with small Hund's exchange coupling where both spin- and orbital degrees of freedom can fluctuate. In a different situation where Hund's exchange coupling is large, a fer-

romagnetic arrangement of spins is favored — here depending on which exchange mechanism is dominant, either an orbital singlet phase, or a non-dimerized phase characterized by local *avoided-blocking* constraints, were identified,^{10,11} but several questions were left open about the precise nature of each phase.

The aim of this article is to understand the effects of the competition between different exchange mechanisms naturally coexisting in such systems, by studying a microscopic orbital model and deriving effective Hamiltonians in extreme regimes. In Sec. II we define the orbital model and analyze its low-energy spectrum and some observables to identify three regimes with distinct ground state properties. Then we analyze the regime where superexchange dominates in Sec. III. This leads us to derive and analyze, in Sec. IV, an effective QDM which allows us to characterize the corresponding phase as an orbital valence bond crystal (VBC). Later on, in Sec. V, we focus on the opposite regime, where direct exchange dominates, and identify by several approaches an exotic phase, fluctuating and with long-range orbital order. Eventually we summarize these findings in Sec. VI.

II. MODEL AND GENERAL APPROACH

A. Model definition

We investigate an orbital model on a triangular lattice, with exactly one electron per site and t_{2g} orbital degrees of freedom. This model is a particular case of the one introduced in Ref. 10 to describe the limit of strong Coulomb interactions in layered, orbitally degenerate transition metal oxides, for instance the Mott insulating titanate NaTiO_2 . In this compound, each titanium ion has a nominal valence $3+$, corresponding to a single electron in the $3d$ shell; due to the crystal field resulting from the octahedron formed by nearest neighbor oxygens, this electron is confined to the t_{2g} subspace of this shell, characterized by the canonical basis: $\{|yz\rangle, |xz\rangle, |xy\rangle\}$. In the present layered structure we can consider a single $[111]$ plane of the NaTiO_2 crystal, with t_{2g} electrons described by a model treating the combined effects of hoppings and Coulomb interactions on a triangular lattice.

A general formulation of the electron dynamics and correlations requires a multiorbital Hubbard model,^{6,10} taking into account all t_{2g} orbitals and spin degrees of freedom. For convenience, in the following we label each bond direction with an index $\gamma \in \{a, b, c\}$ corresponding to the plane (respectively yz, xz and xy) in which the bond is embedded. Kinetic terms are of two types: (i) direct hopping between ions neighboring on the triangular lattice, with amplitude t' — there, the electron can hop only between orbitals of a single flavor, depending on the direction of the bond [this flavor is e.g. $xy \equiv c$ for a bond in the xy plane of the cubic lattice, see Fig. 1(a,b)] — in consequence we rename the orbital flavor allowing for direct hopping in this direction with the same index,³ that is

$$|a\rangle \equiv |yz\rangle, \quad |b\rangle \equiv |xz\rangle, \quad |c\rangle \equiv |xy\rangle; \quad (1)$$

(ii) indirect hopping with amplitude t , where an electron hops,

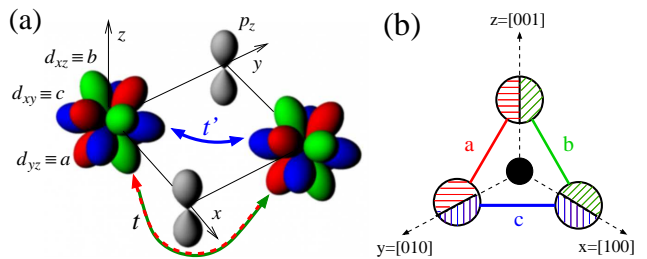


FIG. 1: (Color online) (a) Representation of orbitals on two Ti ions, neighboring on a c -bond, and of the two distinct hopping processes between them: direct hopping of amplitude t' , and indirect hopping - via p_z oxygen orbitals, with amplitude t . (b) An elementary triangle embedded in a $[111]$ plane; each bond of this triangle has a label $\gamma \in \{a, b, c\}$ which labels both the bond direction and [as indicated in Fig. 1(a)] the orbital flavor active in direct exchange on this bond.

from a Ti ion, first to a neighboring oxygen and then to another Ti ion, neighbor of the former on the triangular lattice. This latter hopping process involves exclusively the two orbital flavors not involved in direct hopping on this bond; more precisely, considering two ions neighboring on a c bond, an electron initially in the a orbital of one ion can hop with indirect hopping only to the b orbital of the other ion, and vice-versa [see Fig. 1(a)]. Independently, the on-site Coulomb interactions are governed by Hubbard and Hund's exchange parameters U and J_H , respectively.

In the limit where these interaction amplitudes are larger than hopping parameters, the $3d$ electrons localize and the system is Mott insulating. In this regime of parameters one can use an effective model acting within the subspace with one electron per site (in the present case of d^1 configuration of Ti^{3+} ions), which describes interactions between their spin and orbital degrees of freedom. Such a model was derived for layered titanates in a previous work, see Ref. 10, and contains layered exchange couplings. These follow from second-order processes where one electron hops from a site (Ti ion) to a neighboring site which becomes doubly occupied at an energy cost given by a linear combination of U and J_H , before one of the two electrons hops to the site left empty. The coexistence of direct- and indirect- hoppings implies that three exchange mechanisms are allowed. We list them below, indicating how their amplitudes depend on the hopping parameters t, t' :

- (i) direct-exchange terms which result from processes where both hopping processes involved are direct hoppings, and are thus of amplitude $\propto t'^2$;
- (ii) superexchange terms resulting from processes where both hoppings involved are indirect hoppings, and have an amplitude $\propto t^2$; and finally
- (iii) mixed-exchange terms resulting from processes that combine one direct hopping and one indirect hopping, and their amplitude is thus $\propto tt'$.

These exchange terms couple both spin and orbital degrees of freedom of nearest neighbor (n.n.) ions on a bond $\langle ij \rangle$. As a consequence of the $SU(2)$ -symmetry in spin space of the original Hubbard model, each of them can be written as the

sum of a term with a projection operator ($\vec{S}_i \cdot \vec{S}_j - \frac{1}{4}$) on a spin singlet state on the bond $\langle ij \rangle$, and a term with a projection operator ($\vec{S}_i \cdot \vec{S}_j + \frac{3}{4}$), selecting a triplet state for this bond.

We now specify further the context to a situation with large Hund's exchange coupling J_H (i.e., close to its maximal allowed value $U/3$), when only spin triplet states contribute to exchange processes. This favors the alignment of spins into a ferromagnetic phase, where exchange terms act only on orbital degrees of freedom. This situation can actually also be realized, even if J_H alone is not large enough to polarize spins, in the presence of an external magnetic field, the effect of which adds to that of Hund's exchange — for NaTiO₂ the estimated value of $\eta = J_H/U$ is $\eta \simeq 0.14$, i.e., not far from the value of the estimated transition to the spin-polarized phase $\eta_c \simeq 0.16$.¹¹ In such a spin-polarized phase, setting $J = (t^2 + t'^2)/(U - 3J_H)$ as the unit of energy ($J = 1$), the effective exchange Hamiltonian for orbital degrees of freedom is:

$$\mathcal{H} = (1 - \alpha)H_s + \sqrt{\alpha(1 - \alpha)}H_m + \alpha H_d, \quad (2)$$

where H_s , H_d and H_m are, respectively, the superexchange, the direct exchange and the mixed exchange Hamiltonians defined below. The parameter

$$\alpha = \frac{t'^2}{t^2 + t'^2} \quad (3)$$

interpolates continuously between the superexchange (H_s , for $\alpha = 0$) and direct exchange (H_d , for $\alpha = 1$) Hamiltonians — while the additional mixed-exchange term H_m is present only for $0 < \alpha < 1$, in combination with the others two. The three terms of Eq. (2) are given by:

$$H_s = 2 \sum_{\langle ij \rangle \parallel \gamma} \left\{ (T_{i\gamma}^+ T_{j\gamma}^+ + \text{c.c.}) + \sum_{\mu \neq \gamma} n_{i\mu} n_{j\mu} \right\}, \quad (4)$$

$$H_m = - \sum_{\langle ij \rangle \parallel \gamma} \sum_{\mu \neq \gamma} (T_{i\mu}^+ T_{j\mu}^+ + \text{H.c.}), \quad (5)$$

$$H_d = 2 \sum_{\langle ij \rangle \parallel \gamma} n_{i\gamma} n_{j\gamma}. \quad (6)$$

The electron creation operator in orbital $\gamma = a, b, c$ at site i is γ_i^\dagger , $n_{i\gamma} \equiv \gamma_i^\dagger \gamma_i$, and the single-occupancy local constraint reads $\sum_\gamma n_{i\gamma} = 1$. The notation $\langle ij \rangle \parallel \gamma$ indicates that a bond between sites i and j is oriented along the lattice direction γ , see Fig. 1(b); in other words, this bond is parallel to the vector \vec{e}_γ defined by $\vec{e}_c = (1, 0)$, $\vec{e}_{a/b} = (\pm 1/2, \sqrt{3}/2)$ [see Figs. 2(a) and 2(b)]. In the expressions of super- and mixed exchange terms we use pseudospin operators $\vec{T}_{i\gamma}$ defined for each site *and* flavor index; for instance for $\gamma = c$:

$$T_{ic}^z \equiv \frac{1}{2} (n_{ia} - n_{ib}), \quad (7)$$

$$T_{ic}^+ \equiv a_i^\dagger b_i = (T_{ic}^-)^\dagger. \quad (8)$$

The operators \vec{T}_{ia} and \vec{T}_{ib} are obtained by cyclic permutation of flavor indices. The orbital flavor active in direct exchange

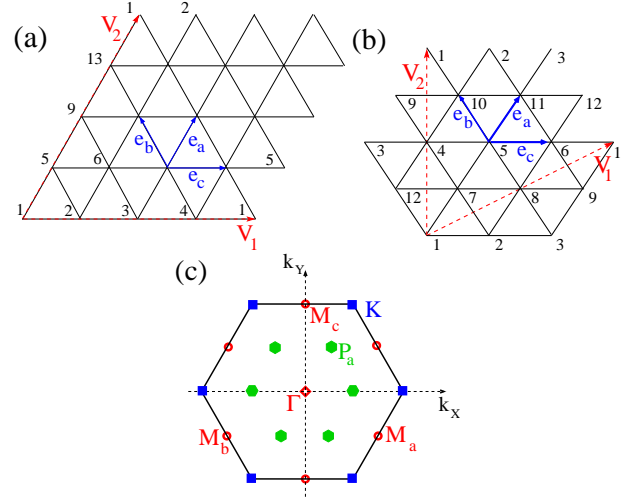


FIG. 2: (Color online) Clusters used for the numerical study of the orbital Hamiltonian Eq. (2), with: (a) $N = 16$ sites and (b) $N = 12$ sites. The multiple occurrence of site indices indicates the periodic boundary conditions, i.e., invariance under translations by vectors $\vec{V}_{1/2}$. (c) First Brillouin zone of the triangular lattice, with Γ , $K = 2P_a$ and $M_{a/b/c}$ points shown — $M_c = (0, 2\pi/\sqrt{3})$ in terms of (k_x, k_y) coordinates.

for each bond direction is depicted in Fig. 1(b); in superexchange on the same bond, both other flavors (and only those) are active. In Eqs. (4) and (5) $\mu\gamma$ is the flavor index distinct from both μ and γ .

B. Numerical analysis of the low-energy spectrum

The Hamiltonian \mathcal{H} [Eq. (2)] is studied by Lanczos exact diagonalization (ED) on periodic clusters. Most generally, these are characterized by two (linearly independent) vectors \vec{V}_1 and \vec{V}_2 : those with the smallest possible value of $|\vec{V}_1 \times \vec{V}_2|$ such that the image of any site by either of these vectors is identified to this site by periodicity. We choose to consider clusters invariant under point group symmetries of the triangular lattice; for this, the simplest choice of vectors \vec{V}_i is e.g. $\vec{V}_1 = L \cdot \vec{e}_c$, $\vec{V}_2 = L \cdot \vec{e}_a$, which corresponds to a $N = L^2$ -site cluster as in the case $N = 16$, see Fig. 2(a). Another possible choice is to take $\vec{V}_{1/2} = L \cdot (\vec{e}_a + \vec{e}_{c/b})$; the corresponding cluster has $N = 3L^2$ sites; we will use hereafter the $N = 12$ cluster shown in Fig. 2(b) (and similar but larger clusters in Sec. IV).

The momentum-resolved low-energy spectrum gives the energy E_0 of the ground state, found at the Γ point. The α dependence of E_0 , see Fig. 3(a), shows a striking contrast between the two opposite regimes: (i) $\alpha \leq 0.6(1)$ where E_0 increases linearly with α , and (ii) α close to 1, where the α -dependence of E_0 is $\propto \sqrt{1 - \alpha}$ [see inset in Fig. 3(a)]. The latter scaling indicates that the low-energy dynamics is here dominated by mixed-exchange terms.

Considering low-energy excitations shown in Fig. 3(b), one notices an intermediate regime (iii) for $0.6 \lesssim \alpha \lesssim 0.8$, where

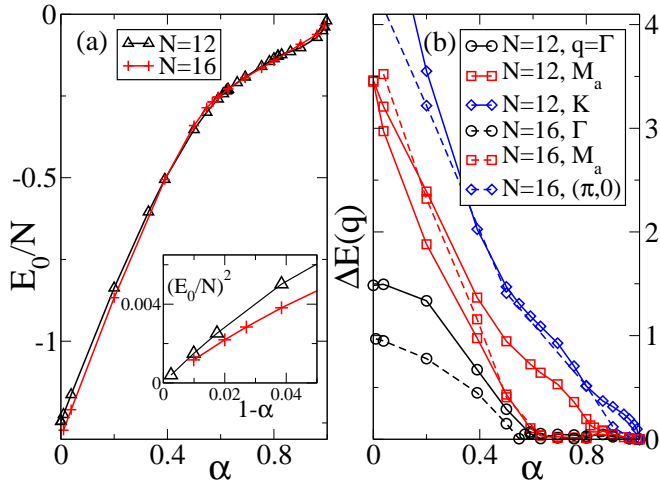


FIG. 3: (Color online) (a) Ground state energy per site E_0/N as function of α for periodic clusters of $N = 12$ and 16 sites. Inset: square of the previous quantity as function of $(1-\alpha)$ in the vicinity of $\alpha = 1$. (b) Lowest excitation energies $\Delta E(\vec{q})$ for momenta $\vec{q} = \Gamma, M_a$, and (depending on cluster size) either K or $(\pi, 0)$, see Fig. 2(c).

several quasi-degenerate lowest states at Γ and M_γ points are well separated from higher excitations. We checked that there are exactly six such low-energy states. Three of them, at the Γ point, consist of a pair of exactly degenerate states, which are the exact ground states for a finite range of α in this regime,²³ and a third low-energy state which is the lowest otherwise. The boundaries $\alpha_{cr,\pm}$ of the zone with exact ground state degeneracy depend slightly on cluster size, e.g. the upper boundary is $\alpha_{cr,+} \simeq 0.81(1)$ and $0.72(1)$ for $N = 12$ and $N = 16$ respectively. The three remaining low-energy states are degenerate, one being at each M_γ point. These features indicate a gapped, ordered phase with six-fold degeneracy of the ground state in the thermodynamic limit (TL).

In contrast, in regime (ii), although lowest states are also found at Γ and M_γ points indicating a symmetry-broken phase, above them, excited states of energy $\sim c_{N,\vec{q}}\sqrt{1-\alpha}$ are compatible with modes becoming gapless in the TL — for details see discussion in Sec. V. Eventually, for $0 \leq \alpha \lesssim 0.6(1)$, the lowest excitations are at the Γ point and have energies $O(1)$ decreasing with increasing N , compatible with an order breaking non-translational symmetries. Note, however, that since both clusters considered are of moderate size and with different shapes, we cannot characterize this phase from their low-energy spectra alone.

III. DIMERIZATION IN THE SUPEREXCHANGE REGIME

In this Section we focus on the regime where superexchange is the dominant exchange mechanism (i.e., we consider the regime of $\alpha \ll 1$). We will provide, within the orbital model Eq. (2), evidence for a dimerized ground state, which we will study further in the next Section using an effective

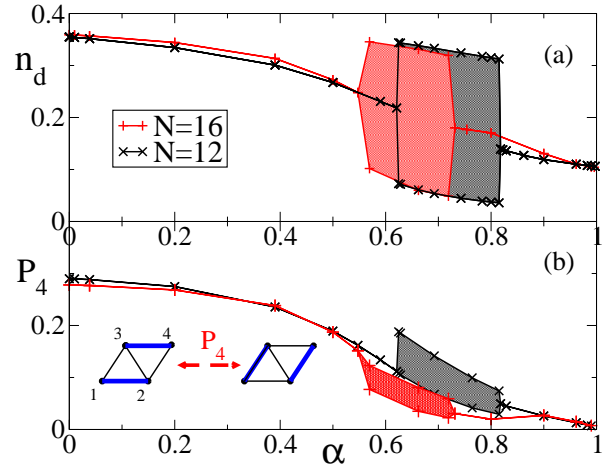


FIG. 4: (Color online) (a) Dimer occupation number $n_d(c)$, and (b) the resonance amplitude P_4 [Eq. (11), with site indices as indicated on the left-hand-side lozenge; each lozenge in the inset shows a singlet covering at play in the resonance] for $N = 12$ and 16 as functions of α . Shaded areas indicate the range of possible values due to an exact twofold ground state degeneracy occurring for both clusters over a finite range of α - see text and Ref. 11.

model.

The superexchange interactions alone, in the present context, are known to favor dimerization into orbital singlets on nearest neighbor bonds.¹⁰ This is clear when one considers an isolated bond $\langle ij \rangle \parallel \gamma$, for which the ground state of H_s is a singlet wave function in terms of the pseudospin variables $\vec{T}_{i,\gamma}$ and $\vec{T}_{j,\gamma}$. On larger systems, we will evaluate the strength of dimerization by computing the dimer or singlet expectation value, defined as:

$$n_d = \langle \Psi_0 | d_{ij}^\dagger d_{ij} | \Psi_0 \rangle, \quad (9)$$

where $|\Psi_0\rangle$ is the ground state found in ED, and

$$d_{ij}^\dagger \equiv \frac{1}{\sqrt{2}} (a_i^\dagger a_j^\dagger - b_i^\dagger b_j^\dagger) \quad (10)$$

is the operator creating a singlet from the electron vacuum for a c -bond $\langle ij \rangle \parallel c$. While for $\alpha \rightarrow 1$ one finds rather small values of $n_d \simeq 1/9$, see Fig. 4(a), a much larger value $\simeq 0.36(2)$ is found for $\alpha \ll 1$, indicating a dimerized ground state. Note that the value $n_d \simeq 1/9$ is close to the values expected for uncorrelated orbitals and almost unaffected by the avoided-blocking constraints. Note as well that the shaded areas in Fig. 4 for $0.6 \lesssim \alpha \lesssim 0.8$ are *not* resulting from computational uncertainty, but from the exact ground state degeneracy occurring in the corresponding (size-dependent) range of parameters. Depending on the actual ground state $|\Psi_0\rangle$ selected within the ground state manifold (here a 2D space), for an observable \mathcal{O} not commuting with \mathcal{H} , $\langle \Psi_0 | \mathcal{O} | \Psi_0 \rangle$ can take all possible values in the range indicated by the shaded area (and delimited by the same symbols as in the non-degenerate case).

Interestingly, the value of n_d obtained for $\alpha \ll 1$ is close to $7/24$ obtained for a variational state $|\Psi_{\text{var}}\rangle$, built as an

equal-amplitude superposition of the twelve columnar singlet coverings which minimize the energy $\langle \Psi_{\text{var}} | H_s | \Psi_{\text{var}} \rangle$ among static singlet coverings. However, the true ground state has a much lower energy and singlet correlations significantly less modulated than those estimated with $|\Psi_{\text{var}}\rangle$, see Appendix A. Hence we compute the quantity:

$$P_4 = \left\langle \Psi_0 \left| (d_{13}^\dagger d_{24}^\dagger d_{12} d_{34} + \text{H.c.}) \right| \Psi_0 \right\rangle, \quad (11)$$

defined on a lozenge and shown as function of α , see Fig. 4(b). A discussion of the value of P_4 on an isolated lozenge and its interpretation in terms of singlet resonance are given in Appendix A. The large values of P_4 shown in Fig. 4(b) for the dimerized ground state of the superexchange regime suggest that it is stabilized by such resonances between nearest neighbor singlets. These resonances can favor either a valence bond crystal (VBC) or a dimer liquid; in the first case large quantum fluctuations may reduce strongly the amplitude of any order parameter related to this order, in comparison with the amplitude expected for a model VBC wave function (such as $|\Psi_{\text{var}}\rangle$ for a columnar phase). Thus, the identification of the phase cannot be addressed directly in ED within the orbital model Eq. (2), but requires to use an adapted effective model, which we describe hereafter.

IV. QUANTUM DIMER MODEL

A. Derivation of a Quantum Dimer Model

Motivated by the evidence discussed above for a dimerized phase in the superexchange regime, we derive a quantum dimer model (QDM) to provide a better understanding of this phase. Such a model, thanks to the reduced number of degrees of freedom at equal size (here the degrees of freedom are not anymore orbital configurations at each site, but the positions of dimers in close-packed dimer coverings fulfilling a hard-core constraint), can be accessed numerically for much larger system sizes than the original orbital model of Eq. (2). It is then possible to address the issue of the behavior in the TL. For this purpose, we follow the Rokhsar-Kivelson (RK) scheme;^{12,22} in the present context this means that we project the orbital Hamiltonian in the subspace spanned by nearest neighbor orbital singlet coverings $|\mathcal{C}\rangle$. An important characteristic of these coverings is that they form an overcomplete, thus non-orthogonal basis. Thus, instead of diagonalizing the Hamiltonian projected onto the singlet coverings' subspace (with matrix elements $\langle \mathcal{C}' | \mathcal{H} | \mathcal{C} \rangle$) one has to solve a generalized eigenvalue problem involving both this matrix and an overlap matrix with elements $\langle \mathcal{C}' | \mathcal{C} \rangle$. Due to the high connectivity of these matrices the numerical solution of this problem is, a priori, much more time consuming than the diagonalization of a sparse matrix of the same size.

An approximation done in similar cases²² consists of expanding the matrix elements mentioned above in powers of a parameter x - here, this parameter is defined formally such that the singlet wave function on a bond $\langle ij \rangle \parallel c$ is $x(|a_i a_j\rangle - |b_i b_j\rangle)$ (similar expressions hold for singlets on

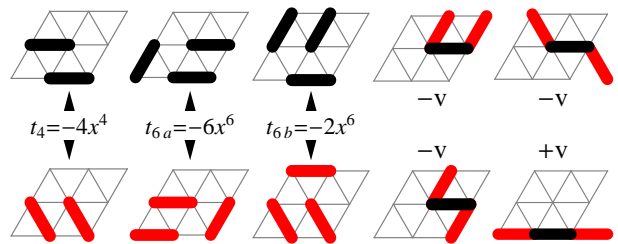


FIG. 5: (Color online) Kinetic processes (three left columns) and configurations with finite potential energies $\lambda_c = \pm v$ (two right columns) in the effective QDM Hamiltonian \mathcal{H}_{QDM} of Eq. (12) derived in the superexchange regime. The coupling between configurations in the leftmost column, with amplitude t_4 , is found at 4th order in overlap expansion, with $x = 1/\sqrt{2}$; subsequent columns show couplings on two inequivalent six-bond loops, with amplitudes t_{6a} and t_{6b} found at sixth order in this expansion. A potential term with amplitudes $\pm v$ applies to every interdimer bond when dimers touching this bond are parallel to each other (the sign depends on whether they are parallel or not to the interdimer bond).

bonds oriented along either \vec{e}_a or \vec{e}_b). Note that, although x takes the value $1/\sqrt{2}$ in the case of interest, here it is introduced as a control parameter for the perturbative expansion. An effective Hamiltonian matrix, in an orthogonal basis of dimer coverings $|c\rangle$ which are in one-to-one correspondence with singlet coverings $|\mathcal{C}\rangle$, is then obtained at given order p of this expansion.

We carried out this derivation up to order $p = 6$, and obtained the following effective Hamiltonian:

$$\mathcal{H}_{\text{QDM}} = \sum_c \lambda_c |c\rangle \langle c| - \sum_{c,c'} t_{c,c'} |c\rangle \langle c'|, \quad (12)$$

where dimer coverings $|c\rangle$ and $|c'\rangle$ differ by a shifted closed loop of length $l = 4$ or 6 . The off-diagonal terms of amplitudes $t_{c,c'}$ and diagonal terms of amplitudes λ_c are explicated below and schematized in Fig. 5; these amplitudes are expressed in units of the superexchange amplitude $J(1 - \alpha)$.

- (a) Off-diagonal (kinetic) terms shown in three first columns of Fig. 5 — each term $\propto |c\rangle \langle c'|$ couples all pairs of dimer configurations which differ from each other *only* by the position of dimers on a short loop of length $l \leq 6$. These terms originate from the off-diagonal part of superexchange interactions on interdimer bonds. The term with amplitude $t_4 = -4x^4$, which flips two dimers on a $l = 4$ -long loop, is found at fourth order in the derivation; at sixth order, two terms flipping three dimers on loops of length $l = 6$ have amplitudes $t_{6a} = 3t_4/4$ and $t_{6b} = t_4/4$, depending on the shape of the loop.
- (b) Diagonal terms $\propto |c\rangle \langle c|$, which play a role of effective potential terms (found at order 4), act on interdimer bonds and favor certain energetically optimal states. These terms originate from the diagonal part of superexchange terms on these bonds. The resulting potential energy λ_c can be written (after a global energy

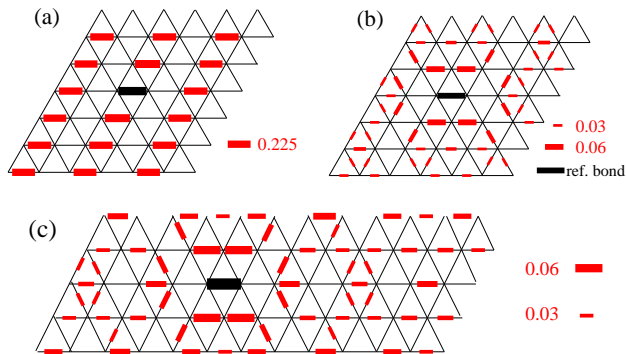


FIG. 6: (Color online) Real-space dimer correlations obtained for the QDM Eq. (12) on periodic clusters: (a,b) on the $N = 36$ cluster, for (a) $v = 1.5$ and (b) $v = 0.5$; and (c) on the $N = 48$ cluster for $v = 0.5$. In (a) correlations correspond to the ground state of the $(1, 1)$ topological sector only, see Sec. IV C.

shift) as a sum over interdimer bonds of terms taking values $\pm v$ when both dimers touching a bond are parallel to each other (see Fig. 5), and 0 otherwise. In the present derivation we have found that $v = t_4/2$.

This effective QDM mimics the accurate properties of the original model in this regime, similarly as in Refs. 8 and 24 for spin-singlet phases. Note that the potential energy is different from the one of the RK QDM on the triangular lattice²⁵ (where it is proportional to the number of lozenges with dimers occupying two parallel edges); here the potential acts on each interdimer bond instead of lozenges.

Although we derived \mathcal{H}_{QDM} for the purpose of studying the superexchange limit $\alpha = 0$, it is also relevant in the regime of $0 < \alpha \ll 1$ where dominant superexchange couplings are perturbed by small mixed-exchange couplings (with amplitude $\simeq \sqrt{\alpha}$). Indeed, matrix elements of the latter do not connect different singlet coverings, thus they do not modify the effective QDM (the direct-exchange perturbation bring some potential terms which, if taken into account, would modify \mathcal{H}_{QDM} , but should be of amplitude $\propto \alpha$ and thus negligible in the limit considered). The main effects of mixed- and direct-exchange terms are to contribute to quantum fluctuations out of the n.n. singlet covering subspace, and to destabilize the dimerized phase for increasing α .

B. Analysis of the quantum dimer model

We have studied \mathcal{H}_{QDM} using two numerical methods: (i) ED on periodic clusters with $N = 12, 36$ and 48 sites — for the largest one the use of translational symmetries and topological invariants (see Sec. IV C) allows us to reduce the Hilbert space size to $N_H \simeq 1.0 \times 10^7$ in a representation of momentum Γ ; and (ii) a zero temperature Green's function quantum Monte Carlo (GFMC).²⁶ This method can be performed here since all the off-diagonal terms are negative. It allows us to obtain the ground states of significantly larger clusters than within ED; here we focus on periodic clusters of

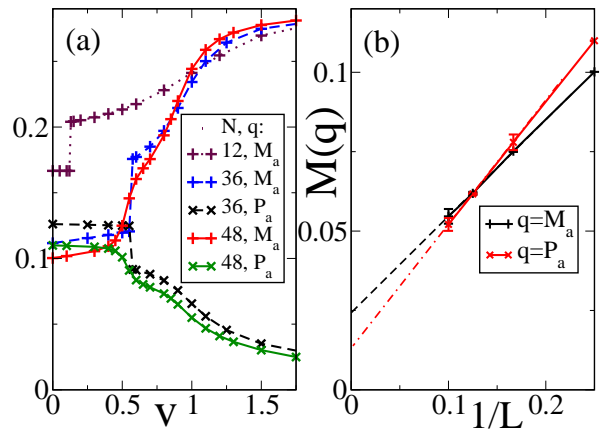


FIG. 7: (Color online) (a) Dimer-dimer order parameter $M(\vec{q})$ [Eq. (13)] at $\vec{q} = P_a$ or $\vec{q} = M_a$ [see Fig. 2(c)] as function of v obtained from ED on clusters of $N = 12, 36$ and 48 sites. (b) Scaling of $M(\vec{q})$ (obtained from GFMC) with inverse linear size for $v = 0$, and either $\vec{q} = M_a$ (circles) or $\vec{q} = P_a$ (squares); dashed lines are a guideline to the eye.

$N = 3L^2$ sites up to $L = 10$. We choose to set, unless they are explicitly specified, the amplitudes of off-diagonal terms to their values obtained in the derivation, and adopt t_4 as unit of energy in this section. But we keep v as a free parameter — this choice allows us to compare the case of interest ($v = 0.5$, corresponding to the superexchange limit $\alpha = 0$ of the orbital model) to two limiting cases that are easier to characterize, and which we address first: (i) $v \gg 1$ and (ii) $|v| \ll 1$.

In case (i), for $t_{c,c'} \equiv 0$ the potential energy is minimized by $O(2^L)$ degenerate ground states (maximally flip-pable states²⁷). Once quantum fluctuations are turned on via $t_{c,c'} \neq 0$, this degeneracy is lifted and a particular ordered phase is selected by a quantum order-by-disorder mechanism;²⁵ for $|t_{6b}| < |t_{6a}|$ one finds²⁸ a columnar VBC. In particular, for $t_{6b} = t_{6a}/3 = 1/4$, this is confirmed by the real-space correlations depicted in Fig. 6(a) on a 36-site cluster and at $v = 1.5$; these correlations clearly indicate a columnar pattern.

More quantitatively, the associated translational symmetry breaking is reflected by a Bragg peak, at points $\vec{q} = M_\gamma$ of the Brillouin zone, in the dimer-dimer order parameter

$$M(\vec{q}) = \frac{1}{N} \left\langle \left\langle \Phi_0 \left| \sum_{i,j,\gamma} e^{i\vec{q} \cdot (\vec{r}_i - \vec{r}_j)} d_{i,\vec{e}_\gamma} d_{j,\vec{e}_\gamma} \right| \Phi_0 \right\rangle \right\rangle^{1/2} \quad (13)$$

where $|\Phi_0\rangle$ is the ground state for a cluster considered. Here $d_{i,\vec{e}_\gamma} = 0$ (1), if a dimer is absent (present) on the bond $\langle ik \rangle \parallel \gamma$ such that the image of the site i by the translation of \vec{e}_γ is k . For $v \geq 1.5$ and $N \geq 36$, $M(M_a)$ exceeds 95% of the maximal value $1/\sqrt{12}$ obtained for a fluctuation-free columnar order, see Fig. 7(a); and this order parameter stays unambiguously finite in the TL for $v \geq 1.0(2)$.

For case (ii), dimer correlations suggest a different translational symmetry breaking in the TL, shown in Fig. 6(b,c). The

Bragg peaks in $M(\vec{q})$ found at both M_a and P_a [see Fig. 7(a), and size scaling for $v = 0$ in Fig. 7(b)] clearly indicate an ordered pattern invariant by $2\pi/3$ -rotations, with a 12-site unit cell called a plaquette in the following. This phase has been found to be stabilized by an $l = 4$ -loop kinetic term, either isolated²⁷ or along with moderate $l = 6$ -loop terms bringing extra resonances within a plaquette.⁸ When v increases, $M(P_a)$ decreases gradually, in parallel with the increase of $M(M_a)$, and eventually vanishes in the TL in the range where the large values of $M(M_a)$ indicate a columnar order, see Fig. 7(a). For a value $v \gtrsim 0.5$, one observes in this figure pronounced jumps in both order parameters, and between this value and $v \simeq 0.8$ it is not clear whether both quantities, or only $M(P_a)$, vanish in the TL. This can correspond either to the onset of a RVB spin liquid²⁷ or to a transition point between two distinct VBCs. Unfortunately, for $v \gtrsim 0.6$ the GFMC suffers from a lack of convergence, which restricts the available cluster sizes,^{8,27} while the correlations obtained by ED are more consistent with a columnar phase.

C. Topological gap

We also discuss the behavior as function of v of another quantity easily obtained within the effective QDM: the so-called *topological gap* ΔE_t ,^{22,25,29} which is well defined on a periodic system, e.g. a torus, for a QDM where off-diagonal terms correspond only to local updates (this is the case here). On a torus accommodating the rotation symmetries of the lattice, it is defined as follows,

$$\Delta E_t = |E_0(W_c = W_a = 1) - E_0(W_c = W_a = -1)|, \quad (14)$$

where $W_\gamma = (-1)^{n_\gamma}$ are topological invariants, such that n_γ is the number of dimers crossing a line parallel to the γ axis and winding around the torus. Since the parity of n_a and n_c is conserved by all kinetic terms of the QDM, each topological sector, or subspace spanned by all dimer configurations with fixed W_a and W_c , is well-defined. We also remark that, on clusters invariant by point group symmetries of the triangular lattice, the two sectors such that $W_a + W_c = 0$ have the same spectrum as either the $W_a = W_c = -1$ sector, or the $W_a = W_c = 1$ one, depending on the cluster size.

The topological gap provides valuable insights into the nature of the ground state. In a VBC this gap grows as the linear size L of the system. This is because the ordered pattern fits in only one of the two topological sectors $(W_a, W_c) = (1, 1)$ and $(-1, -1)$; and ΔE_t corresponds to an excitation disturbing the crystalline order over a whole winding loop. On the contrary, in a dimer liquid all topological sectors are fully equivalent in the TL and the topological gap is simply a finite-size effect, e.g. for a gapped \mathbb{Z}_2 liquid it behaves as $L^\delta e^{-L/\xi}$, with $\xi > 0$ and δ a constant depending on the parity of $L/2$.²⁷

In the present case, on a large cluster of size $N = 3L^2$ [see Fig. 8 with $L \leq 8$], ΔE_t decreases linearly with v from a finite value at $v = 0$ [expected in a plaquette phase where the ground state is in the sector $(W_c = W_a = (-1)^{L/2})$] down to almost zero for $v_c = 0.55(5)$. When v increases further

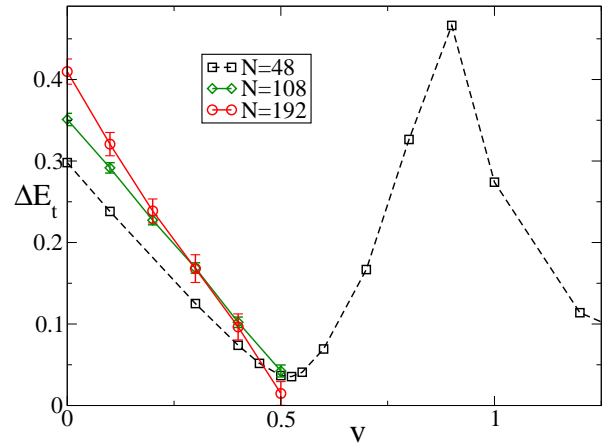


FIG. 8: (Color online) Topological gap ΔE_t [Eq. (14)] versus v obtained for the QDM using large clusters of $N = 3L^2$ sites with periodic boundary conditions. The data are obtained by exact diagonalization for $L = 4$ and with quantum Monte Carlo for $L \geq 6$.

it takes again a finite value in the columnar phase: here, the ground state is found in the sector $(W_c = W_a = 1)$ (and, if $L/2$ is odd, also in sectors such that $W_c = -W_a$). Thus, when going from one phase to another, depending on the parity of $L/2$ the ground state changes or not its topological sector; we have verified that the value of v minimizing $\Delta E_t(v)$ is roughly independent of L , so that this minimum is a good indicator for the transition. In contrast, the maximum of $\Delta E_t(v)$ for $v \simeq 0.9$ in the $N = 48$ case merely signals a crossing between a non-local excitation of energy $\Delta E_t \propto 1/v^3$ (as expected from perturbation theory in the large v regime) and another non-local excitation which is of lower energy close to the transition to the plaquette phase, where this excitation energy vanishes. From this data the hypothesis of an intermediate RVB phase, in which Δ_t extrapolated to the TL would vanish in a finite range of v , seems unlikely. Besides, the vanishing of the topological gap observed for $v_c \simeq 0.55(5)$ coincides with the changes occurring in the dimer order parameter.

Although we cannot exclude a liquid phase stabilized in a narrow range of $v \simeq 0.5$, the most probable scenario is thus a first order transition between plaquette and columnar phases, occurring at $v \simeq 0.55(5)$; this implies that the former phase is expected to be stabilized in the superexchange regime.

V. THE DIRECT EXCHANGE REGIME

We concentrate now on the regime $\alpha > 1/2$ of the model, where direct exchange is dominant. For $\alpha \rightarrow 1$ all other couplings can be treated as perturbations and, as we did in the previous sections, it is again possible to derive an effective Hamiltonian which correctly captures the ground state properties of the microscopic system. In the following, we report the presence of an exotic ground state in this regime, and propose a complete analysis for its characterization.

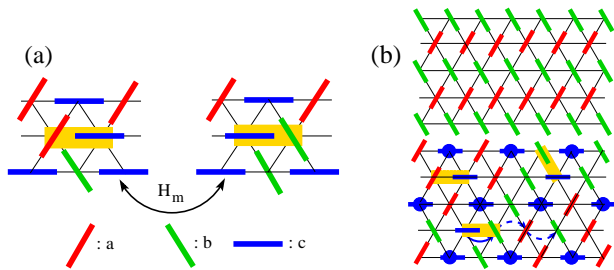


FIG. 9: (Color online) Orbital states for $\alpha \simeq 1$: (a) typical mixed-exchange process connecting two avoided-blocking states, which differ on the shaded bond; (b) ordered patterns — the purely collinear pattern (top) is frozen for $\alpha \rightarrow 1$, while the other (bottom) allows for low-energy dynamics on the highlighted bonds by consecutive processes triggered by mixed-exchange terms (arrows), whereas one sublattice (marked by full dots) is ordered.

A. Effective model within the *avoided-blocking* subspace

We start from the limit $\alpha \equiv 1$, in which $\mathcal{H} \equiv H_d$ is positively definite and selects a macroscopically degenerate ground state manifold, characterized by $n_{i\gamma}n_{j\gamma} = 0$ on every bond $\langle ij \rangle$ parallel to \vec{e}_γ . These orbital configurations, called *avoided-blocking* states, can be described in a representation where a rectangle at each site of the triangular lattice represents the orientation of the occupied orbital at this site — a rectangle parallel to γ -bonds (but centered on the site i , in contrast to dimers of Sec. IV which were centered on bonds) means that $n_{i,\gamma} = 1$ in the configuration considered here, see Figs. 9(a) and 9(b). The number of such configurations grows exponentially with system size, i.e., they are macroscopically degenerate and form a low-energy subspace separated from higher-energy configurations by a gap $\simeq 2\alpha \simeq 2$ in this limit. Close to this limit (for $0 < 1 - \alpha \ll 1$) the weight of other configurations, with *blocking defects* — consisting on bonds $\langle ij \rangle \parallel \gamma$ where on both sites i and j the γ orbital is occupied — is proportional to $1 - \alpha$. This scaling can be easily understood within second order perturbation theory where mixed-exchange terms, which can create/annihilate such defects, are treated as perturbations w.r.t. direct exchange.

In this regime, the ground state is thus mostly composed of avoided-blocking configurations, and its properties are determined by the action of mixed-exchange (and to a lesser extent of superexchange) perturbations within the avoided-blocking subspace. Indeed, as shown in Fig. 9(a) a single mixed-exchange term can connect distinct avoided-blocking states, allowing for important quantum fluctuations. We investigate whether fluctuations can account for a disordered ground state, or whether the perturbing exchange terms select a long-range orbital order, by a quantum order-by-disorder mechanism. To that extent, we define and consider an effective Hamiltonian, found at first order in a perturbation theory where super- and mixed exchange are considered as perturbations to the direct exchange Hamiltonian:

$$H_{\text{eff}} \equiv \sqrt{1 - \alpha} \left(\sqrt{1 - \alpha} \mathcal{P} \mathcal{H}_s \mathcal{P} + \sqrt{\alpha} \mathcal{P} \mathcal{H}_m \mathcal{P} \right). \quad (15)$$

Here \mathcal{P} is the projection operator onto the avoided-blocking subspace, i.e., in the basis of orbital configurations $\{|c\rangle\}$ (eigenstates of all $\gamma_i^\dagger \gamma_i$ operators), $\mathcal{P}|c\rangle = |c\rangle$ if $|c\rangle$ is an avoided-blocking configuration, while $\mathcal{P}|c\rangle = 0$ otherwise.

The ground state $|\Psi_0^{\text{eff}}\rangle$ of H_{eff} can be accessed for significantly larger cluster sizes ($N \leq 36$ sites in Lanczos ED) than the ground state $|\Psi_0\rangle$ of the original Hamiltonian \mathcal{H} ; thus it allows us to address in a more controlled way the possible existence of long-range order in the TL.

B. Orbital ordering

The first quantity we consider to address the possibility of orbital ordering is the structure factor of orbital correlations,

$$S_\gamma(\vec{q}) = \frac{1}{N^2} \sum_{i,j} e^{i\vec{q} \cdot (\vec{r}_i - \vec{r}_j)} \langle \Psi | n_{i\gamma} n_{j\gamma} | \Psi \rangle, \quad (16)$$

choosing for $|\Psi\rangle$ either the ground state $|\Psi_0\rangle$ of the full model or an approximate state $|\Psi_0^{\text{eff}}\rangle$ of the effective model defined in Sec. V A. Due to local constraints imposed by dominating direct-exchange interactions, $S_c(\vec{q})$ is expected to be maximal at M_a and M_b . The type of ordered pattern which maximizes this quantity consists of lines with orbital flavors uniform within a line and alternating between neighboring lines — we call this *collinear order*. On a cluster invariant by point group symmetries, $S_c(M_a) = 1/12$ if $|\Psi\rangle$ in Eq. (16) is chosen as an equal weight superposition of all such patterns (there are six of them, since lines parallel to \vec{e}_γ and containing γ orbitals are forbidden here). Here we find that for α larger than 0.6(1), $S_c(M_a)$ takes values of the same order of magnitude, and the comparison between different clusters [see Fig. 10(a)] indicates that in the TL this quantity may stay finite.

In the limit $\alpha \rightarrow 1$ on which we focus first, this is confirmed by $S_c(M_a)$ obtained from the ground state $|\Psi_0^{\text{eff}}\rangle$ of the effective model H_{eff} , which for $\alpha \rightarrow 1$ reduces to $H_m^{\text{eff}} = H_{\text{eff}}(\alpha \rightarrow 1) \propto \mathcal{P} H_m \mathcal{P}$; Fig. 10(b) clearly indicates that $S_c(M_a)$ computed with $|\Psi_0^{\text{eff}}\rangle$ stays finite in the TL, scaling roughly as $c_1 + c_2/N$ where $c_1 > 0$. Note that its value for e.g. $N = 12$ matches well the one in Fig. 10(a) for the same cluster size and $\alpha \rightarrow 1$; besides, both wave functions $|\Psi_0\rangle$ and $|\Psi_0^{\text{eff}}\rangle$ have there a large mutual overlap $\simeq 1 - k\alpha$. This confirms the validity of the effective model Eq. (15) in this limit, where the ground state is thus characterized by long-range orbital order inducing a translational symmetry breaking in the TL.

A collinear phase would be compatible with such a result: indeed the corresponding ordered patterns [see Fig. 9(b)-top] belong to the avoided-blocking subspace. Yet, the stabilization of this phase is not expected in this limit; collinear ordered patterns do not allow for mixed-exchange fluctuations, whereas these are essential in selecting a ground state with finite and negative $\langle H_m \rangle$ (within the effective model we estimated $\langle H_m \rangle / N \simeq -0.35(5)$ in the TL). With a similar reasoning, one can exclude other candidate phases with static orbital order. A dimerized phase could also be considered as a candidate, since mixed-exchange favors a resonating state on individual bonds, e.g. the resonating state

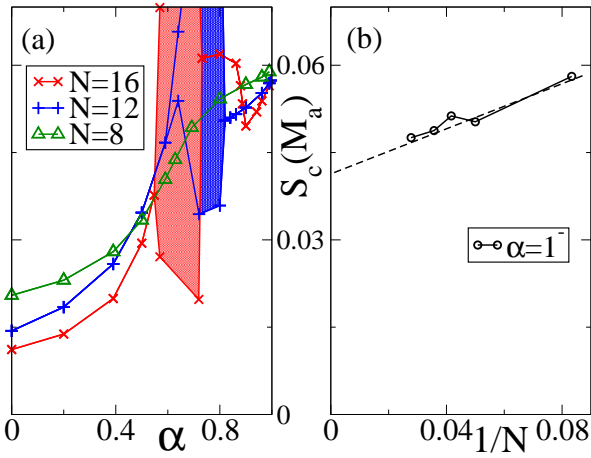


FIG. 10: (Color online) Structure factor $S_c(M_a)$ of orbital correlations, see Eq.(16), as obtained (a) within the orbital model of Eq. (2) for the ground states of $N = 8, 12, 16$ clusters, and for increasing α ; and (b) within the effective model of Eq. (15) for the ground states of $N \leq 36$ clusters, for $\alpha \rightarrow 1$; for computational details see Ref. 30. In (b) the dashed line is a guide to the eyes.

$(1/\sqrt{2})(|c_i a_j\rangle + |b_i c_j\rangle)$ on a bond $\langle ij \rangle \parallel c$; yet such a phase, where blocking defects cannot be avoided, would not be favorable either.

While the nature of the ground state for $\alpha \rightarrow 1$ remains open after the discussion above, one notices that an upturn occurs in $S_c(M_a)$ when α is decreased until reaching a value $\alpha_c \simeq 0.81(1)$ ($\alpha_c \simeq 0.86(2)$) for $N = 12$ ($N = 16$), see Fig. 10(a). This upturn coincides ($N = 12$) or not ($N = 16$) with the boundary of the regime with exact twofold ground state degeneracy; it signals a change in the ground state, which for $\alpha \lesssim \alpha_c$ could be collinear-ordered. Indeed, the diagonal part of superexchange is minimized among avoided-blocking states by collinear patterns, in which e.g. a and b orbitals are never neighboring on a c -bond; far enough from the $\alpha \rightarrow 1$ limit, superexchange becomes nonnegligible compared to mixed exchange and can favor the collinear order.

C. Insights from low-energy excitations

We now analyze, still in the direct-exchange-dominated regime, the low-energy spectra of both the orbital Hamiltonian \mathcal{H} [Figs. 11(a) and 11(b)] and the effective Hamiltonian H_{eff} [Figs. 11(c) and 11(d)]. For α close to 1, as mentioned in Sec. II B, the lowest states are found in representations of momenta Γ and M_γ .³¹ Above them, one notices excitation branches with energy

$$\Delta E(\vec{q}) \simeq c_{N,\vec{q}} \sqrt{1 - \alpha}, \quad (17)$$

i.e., proportional to the amplitude of mixed-exchange processes. In contrast to low-energy states characteristic of a hypothetical gapped, orbital ordered phase evoked earlier, these states are not restricted to high-symmetry momenta, and thus they (or at least some of them) are not a mere consequence

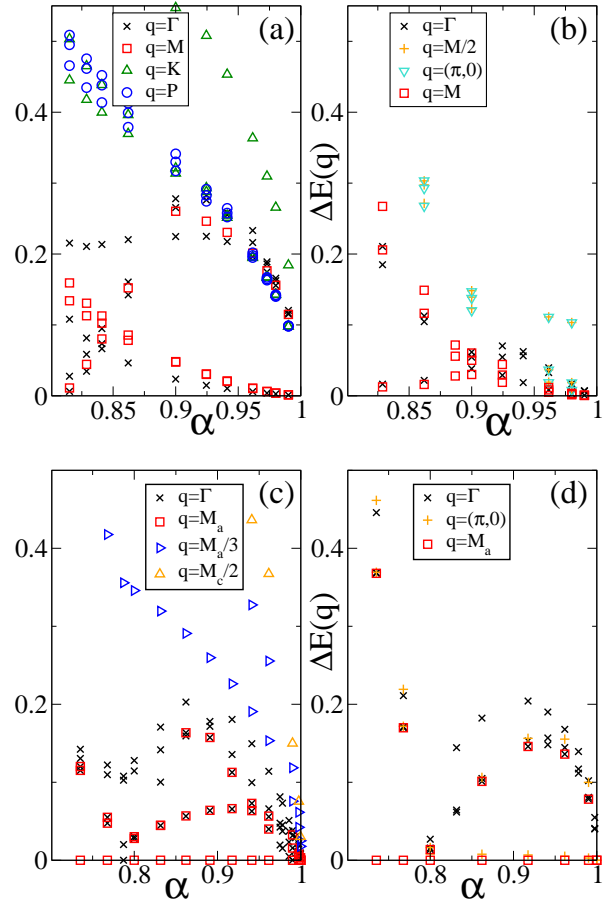


FIG. 11: (Color online) Top part — low-energy spectrum of the orbital Hamiltonian \mathcal{H} in the direct-exchange-dominated regime ($\alpha \geq 0.8$) for clusters of (a) $N = 12$ and (b) $N = 16$ sites. Bottom part — low-energy spectrum of the effective Hamiltonian H_{eff} [Eq. (15)], for $\alpha \geq 0.7$, and clusters of: (c) $N = 24$, and (d) $N = 16$ sites.

of translation symmetry breaking in the TL. When comparing between different sizes the values $\min_{\vec{q}}\{c_{N,\vec{q}}\}$ corresponding to the lowest of these branches (which is typically at Γ and M_γ points) this value decreases significantly with increasing N and seems to vanish in the TL; excitations with a similar scaling law [Eq. (17)] are also found at other momenta — they have energies getting smaller with increasing N . These states may follow a certain dispersion law $\omega(\vec{q})$, quantized here by the finiteness of clusters considered, but corresponding to a gapless mode of this phase.

This situation contrasts with what we see further away from the direct-exchange limit, that is, for $0.6 \lesssim \alpha \lesssim 0.8$ within the effective model — as well as within the full model for the same range of α , see Fig. 3(b). In the latter regime, the spectrum is characteristic of the collinear phase with lowest states *only* at Γ and M_γ , while excitations with other momenta are found at much higher energies. Between both regimes, a level crossing occurs between two groups of quasi-degenerate lowest states, of different nature — on each side of the crossing the number and momenta of lowest states indicate the sym-

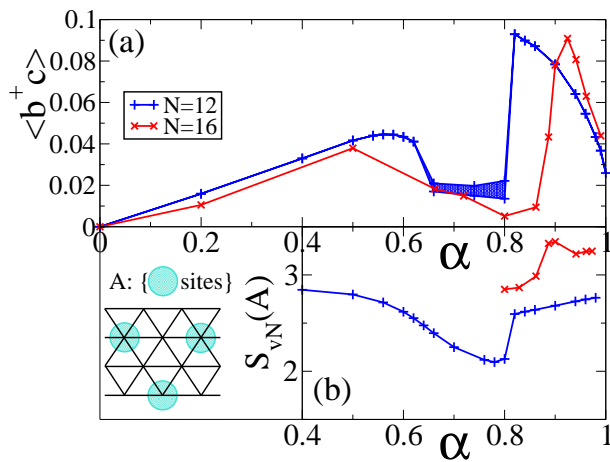


FIG. 12: (Color online) (a) Amplitude of on-site orbital fluctuations $\langle b^\dagger c \rangle$ and (b) von Neumann entanglement entropy $S_{vN}(A)$, both evaluated in the ground state of Eq. (2) for $N = 12, 16$ site clusters³³, as a function of α . The inset shows the subset A of lattice sites used in the definition of $S_{vN}(A)$ [see Eq. (19)].

metries broken in the TL. At equal size, this crossing occurs for a value of α slightly larger in the original model than in the effective model (e.g. for $N = 16$, at $\alpha \simeq 0.9$ and $\simeq 0.8$, respectively). The origin of this difference in the crossing position is that the effective model underestimates effects of off-diagonal superexchange terms which contribute to stabilize the collinear phase. But the crossing position is not much sensitive to the system size (within the effective model, on clusters $N = 12, 16, 20, 24$, this crossing occurs at $\alpha = 0.755(5)$, $0.795(5)$, $0.73(1)$, and $0.79(1)$ respectively). This shows that the effective model Eq. (15) captures well, qualitatively, the transition between the collinear phase found in a regime where super-, direct and mixed exchange amplitudes are comparable, and a phase with a distinct, unconventional orbital order, found in the direct exchange regime i.e. for α close to 1.

D. Strong orbital fluctuations in a symmetry-broken phase

The unconventional structure of the low-energy spectrum observed for $0 < 1 - \alpha \lesssim 0.2$, with possibly gapless excitations, contrasts with the — at least partial — orbital ordering evidenced by large values of $S_c(M_a)$. To understand how these features can coexist, we evaluate, on the ground state of the full model Eq. (2) and for a fixed site i , the amplitude of on-site orbital fluctuations:

$$\langle b^\dagger c \rangle = \langle \Psi_0 | b_i^\dagger c_i | \Psi_0 \rangle, \quad (18)$$

shown in Fig. 12(a). This quantity is remarkably large for $\alpha \geq 0.9$, where it has only weak size-dependence. We checked that on-site orbital fluctuations have comparable amplitudes for larger clusters, if computed within the effective model Eq. (15) in the same range of α . The importance of these fluctuations is consistent with a finite *orbital compressibility*, i.e., the fact that the electron density in γ orbitals can

be tuned continuously by an adapted chemical potential (for details see Appendix B); and with the presumably gapless excitation modes discussed in the previous paragraph.

When α is decreased further away from the direct-exchange limit, a drop in $\langle b^\dagger c \rangle$ occurs simultaneously with the upturn in $S_c(M_a)$ and the crossing in the low-energy spectrum discussed previously. This is a further indication for the transition toward static collinear order for α smaller than this value, while for α close to 1 the mixed-exchange energy stabilizes a qualitatively more fluctuating ground state. From the data of Figs. 3, 10, and 11, one can locate the transition between these two phases at roughly $\alpha \simeq 0.8(1)$.

Another instructive quantity is the von Neumann entanglement entropy between one sublattice and the rest of the system,³² defined as:

$$S_{vN}(A) = -\text{Tr} \{ \rho_A \ln(\rho_A) \}, \quad (19)$$

where ρ_A is the reduced density matrix computed for the ground state of an N -site cluster,³³ corresponding to a partition between an ensemble A of $N/4$ sites forming a triangular sublattice with doubled unit cell [see inset of Fig. 12(b) or Fig. 9(b)-bottom] and the complementary sites, which form a kagome lattice. This quantity, shown in Fig. 12(b), displays a clear jump at the same position (on the α axis) as the jump in $\langle b^\dagger c \rangle$ discussed previously. The entropy $S_{vN}(A)$ is significantly larger on the right hand side of the jump, evidencing here a more fluctuating ground state, than on the left hand side. Besides, we compared this quantity with entanglement entropies corresponding to other partitions; in those cases, we also found jumps at the same value of α , but with smaller amplitudes [e.g. when considering $S_{vN}(B)$ with B being a lozenge of 4 sites, on the $N = 12$ cluster, between $\alpha = 0.8$ and $\alpha = 0.82$ this quantity increases by $\simeq 0.15$ compared to an increase of $\simeq 0.47$ in $S_{vN}(A)$].

These features, in a ground state with spontaneously broken translation symmetry, motivate us to suggest the following scenario: the symmetry breaking corresponding to translations by vectors \vec{e}_γ ($\gamma = a, b, c$) allows the ground state to have a structure where four different sublattices play non-equivalent roles; in a simplified picture [see Fig. 9(b)-bottom] one sublattice is ferro-orbitally ordered, with e.g. c -orbitals covering this sublattice. On other sites, which alone form a kagome lattice, the number of electrons of a given orbital flavor fluctuates mainly via mixed-exchange processes. By these processes, an electron with c orbital flavor can propagate along c bonds as long as it doesn't meet another electron of this flavor; at each step of this propagation, the electron moving in the opposite direction converts its orbital flavor from a to b or vice versa. In other words, such a succession of mixed-exchange processes on neighboring bonds (see plain and dashed arrows in Fig. 9(b)-bottom) can be seen as the effective motion, at arbitrary distance and *without direct-exchange-induced energy cost*, of a single c orbital along a line containing alternating a and b orbitals. Similar effective single-orbital motions are also possible in other directions; the low-energy orbital dynamics are thus not confined in one spatial dimension but rather on an effective kagome lattice. The freezing of the complementary sublattice may be interpreted

as an order-by-disorder effect. One can also note that the lattice symmetry breaking evidenced here has been predicted for interacting t_{2g} electrons in such a geometry, due to the structure of hoppings.³⁴

Altogether, this scenario allows to understand qualitatively that, in the direct-exchange-dominated regime for $\alpha \gtrsim 0.8$, the ground state is characterized by: (i) large on-site orbital fluctuations, (ii) a significantly higher entanglement entropy $S_{vN}(A)$ than in the collinear state favored for smaller α , and (iii) above the former ground state there may be a continuum of low-energy excitations, possibly gapless. This phase would be an orbital analog of a (bosonic) supersolid³⁵ or (fermionic) pinball liquid,³⁶ and is in any case an original and rather exotic type of ground state in the context of orbital models.

VI. SUMMARY AND CONCLUSIONS

In this paper we have addressed a situation where large Coulomb interactions lead, even though the spin degrees of freedom are frozen in a ferromagnetic phase, to a high frustration of effective interactions between t_{2g} orbital degrees of freedom. This is due to two factors: first, even when considered separately, both superexchange or direct exchange interactions are frustrated on the triangular lattice, while analog models on e.g. a square lattice would allow for orbitally ordered ground states; second, in the present model there is a competition between three distinct exchange mechanisms which naturally coexist in the compounds such as NaTiO_2 , motivating this model. To address the nature of the ground states selected by these interactions, we studied both the orbital model itself and two effective models adapted to extreme situations. For these studies we employed numerical techniques — mostly exact diagonalization, extended by Monte Carlo techniques for one of these models. This allowed us to characterize several ground states, depending on the parameter α governing the ratios between amplitudes of the three exchange interactions:

(i) In the regime of dominant superexchange ($\alpha \ll 1$), we found concordancing evidence for a dimerized phase, where electrons pair into orbital singlets on nearest neighbor bonds. The effective quantum dimer model which we derived in this context allowed us to characterize this phase as a plaquette valence bond crystal (VBC) with a large unit cell (of 12 sites), and which is stabilized by resonances between singlets within this unit cell. We also found that slight modifications of interaction parameters might lead to a transition to another, columnar, VBC; this suggests that such a system should remain disordered down to very low temperatures. Yet, the tendency towards dimerization and the mechanism stabilizing the plaquette VBC seem to be robust to small mixed exchange interactions perturbing the superexchange ones, for $\alpha \lesssim 0.6(1)$.

(ii) In the intermediate regime where superexchange, mixed exchange and direct exchange interactions have comparable amplitudes, for $0.6(1) \lesssim \alpha \lesssim 0.8(1)$, we identified a different phase, with *collinear* orbital ordering in lines, where the orbital flavor is uniform within a line but alternates between neighboring lines. This phase, with gapped excitations, seems

to be stabilized by the joined effects of direct exchange and superexchange interactions — the former select a large number of low-energy orbital configurations (*avoided-blocking states*), among which those favored by superexchange couplings are the collinear patterns.

(iii) Eventually, in the third regime, for $\alpha \gtrsim 0.8(1)$ where direct exchange is by far the dominant exchange mechanism, we found an original type of ground state, resulting from the action of subdominant mixed exchange interactions within avoided-blocking states. This ground state is characterized by a spontaneous symmetry breaking, which allows for a structure where orbital long-range order and strong orbital fluctuations develop on distinct sublattices; the corresponding phase has low-energy modes, presumably gapless, within the avoided-blocking subspace. The spatial ground state structure indicated by our results suggests that it might be an original realization of supersolid- or pinball-like behavior in orbital physics.

Based on these findings, several open questions are left for future studies: in the superexchange-dominated regime, the proximity to the columnar-plaquette transition within the effective dimer model we considered indicates that a refined dimer model, including terms found at further order in the overlap expansion, might predict a columnar ground state, or even a third dimerized phase, for the superexchange regime. In the direct-exchange-dominated regime, it would also be valuable to confirm — or invalidate — our scenario by complementary techniques, ranging from mean field approaches to variational techniques, applied either to the orbital model or to the effective model adapted to this regime. Independently from these issues, one could also investigate whether the phases we evidence here might be realized in existing compounds — for this purpose one should include small octahedral distortions (which exist in NaTiO_2 [37]) along with the various exchange couplings considered here. An investigation of properties of the resulting orbital model, if compared to hypothetical (e.g. thermodynamic, or of resonant inelastic x-ray scattering) measurements on titanates in high magnetic fields, would allow to estimate the relative amplitudes of the different exchange mechanisms; one could then consider these amplitudes (or this value of α) and focus on the low-field regime, to study the possibility of a spin-orbital liquid phase.

Acknowledgments

We thank G. Jackeli and K. Penc for insightful discussions, and J. Chaloupka for discussions and technical assistance. We acknowledge support by the European Science Foundation (Highly Frustrated Magnetism, Grant No. 2525) (F.T.), the French National Research Agency, Grant No. ANR 2010 BLANC 0406-0 (A.R.), and the Polish National Science Center (NCN) under Project No. N202 069639 (A.M.O.). A.R. thanks CIMENT cluster facilities (Grenoble, France) for computation time.

Appendix A: Resonance processes in the superexchange limit

In the superexchange regime, for $0 \leq \alpha \ll 1$, the tendency toward dimerization is quite strong and favors *a priori* a large number of nearest neighbor orbital singlet coverings, where a singlet is created (from the vacuum) by the operator d_{ij}^\dagger on a bond $\langle ij \rangle$ — for instance, for a bond $\langle ij \rangle \parallel a$,

$$d_{ij}^\dagger \equiv \frac{1}{\sqrt{2}} (b_i^\dagger b_j^\dagger - c_i^\dagger c_j^\dagger). \quad (\text{A1})$$

Distinct singlet coverings arise naturally due to the form of H_s and are non-orthogonal to one another. In a dimerized phase, the ground state composed of these coverings may undergo resonances which lower its energy and determine the orbital correlations. To quantify the importance of resonance processes between different singlet coverings we define the quantity P_4 related to resonances on the smallest non-trivial loop, that is on a lozenge. By labeling sites on a lozenge in a way shown in Fig. 4, this quantity reads as:

$$P_4 = \langle \Psi_0 | d_{13}^\dagger d_{24}^\dagger d_{12} d_{34} + d_{12}^\dagger d_{34}^\dagger d_{13} d_{24} | \Psi_0 \rangle, \quad (\text{A2})$$

where $|\Psi_0\rangle$ is the ground state found in exact diagonalization on the cluster considered. Typical values of P_4 are $P_4 \simeq 0.29(2)$ in the superexchange limit $\alpha = 0$, as seen in Fig. 4(b), and decrease with increasing α in the same way as the dimer expectation value n_d . This indicates that, while fluctuations out of the dimerized subspace increase, the resonance processes stabilizing the dimerized phase subsist until this phase becomes less favorable than a non-dimerized phase. The values found on $N = 12, 16$ clusters can be compared to the extreme (maximal) value corresponding to a 2×2 cluster, where such a resonance (or flip) affects the whole system. Assuming here again periodic boundary conditions (so that all orbital flavors are equivalent), one can easily check that the ground state of this cluster at $\alpha = 0$ reads:

$$\begin{aligned} |\Psi_0^{\alpha=0}\rangle &= \frac{1}{\sqrt{6}} \left\{ |a_1 a_2 a_3 a_4\rangle + |b_1 b_2 b_3 b_4\rangle + |c_1 c_2 c_3 c_4\rangle \right\} \\ &- \frac{1}{\sqrt{12}} \left\{ |a_1 a_2 b_3 b_4\rangle + |b_1 b_2 a_3 a_4\rangle + |a_1 c_2 c_3 a_4\rangle \right. \\ &\left. + |c_1 a_2 a_3 c_4\rangle + |b_1 c_2 b_3 c_4\rangle + |c_1 b_2 c_3 b_4\rangle \right\}, \quad (\text{A3}) \end{aligned}$$

and from this it follows that

$$P_4 = \frac{1}{2} + \frac{\sqrt{2}}{3} \simeq 0.971. \quad (\text{A4})$$

Such a large value cannot be expected on significantly larger clusters, where resonances on lozenges coexist with resonances on loops of length $l \geq 6$; but even there, values $P_4 \simeq 0.29(2)$ for $\alpha \rightarrow 0$ prove that the contribution of such resonances to orbital dynamics is significant in this regime, leading to the ground state energy per site $E_0 \simeq -1.25(5)$. Note that this energy is much lower than expected for a static singlet covering. In fact, the superposition $|\Psi_{\text{var}}\rangle$ of columnar singlet coverings has an energy per site,

$$\langle \Psi_{\text{var}} | H_s | \Psi_{\text{var}} \rangle = -0.5. \quad (\text{A5})$$

Appendix B: Influence of an external chemical potential in the direct-exchange regime

An interesting aspect shedding light onto ground state properties for $\alpha \rightarrow 1$ is its sensitivity to an external orbital field, or chemical potential, distinguishing one type of orbital (say, c ones) from the two others. The effective model augmented by this potential reads now:

$$H_{\text{eff},c} = H_{\text{eff}} + \mu_c \sum_i n_{i,c}. \quad (\text{B1})$$

Similarly, within the full orbital model, one can add such a chemical potential of amplitude μ_c . When this one is positive and large compared to the mixed-exchange amplitude $x_m = \sqrt{\alpha - \alpha^2}$, the chemical potential selects, among avoided-blocking configurations, those which minimize (to zero) the population of c orbitals defined as

$$n_c = \frac{1}{N} \sum_i \langle \Psi_0 | n_{i,c} | \Psi_0 \rangle. \quad (\text{B2})$$

The selected configurations are two collinear states with alternating rows of a and b orbitals, see Fig. 9(b)-top. For $\mu_c \ll -x_m$ (but both quantities small before the direct-exchange amplitude), the chemical potential favors the four other collinear states, obtained from the two previous ones by a lattice rotation combined with a flavor permutation, and now maximizing n_c within the avoided-blocking subspace. We show in Fig. 13 the dependence of n_c on μ_c within the constrained model $H_{\text{eff},c}$ in the direct-exchange limit $\alpha \rightarrow 1$, as well as within the full orbital model for two values, small but finite, of $1 - \alpha$.

Instead of a direct transition between the two ordered regimes mentioned above, characterized respectively by $n_c = 0$ and $n_c = 1/2$ up to quantum fluctuations, we observe an intermediate regime where n_c varies continuously with μ_c . In this regime, the ground state has a finite *orbital compressibility* (defined here as $\frac{dn_c}{d\mu_c}$). When the mixed-exchange amplitude x_m is small, the values of the chemical potential corresponding to transitions from the intermediate regime to both collinear ordered ones, $\mu_{c,\pm}$ [see Fig. 13 for $\mu_{c,+}$], are close to $\pm x_m$. When α is decreased, one sees that $\mu_{c,+}$ decreases slightly — this behavior is consistent with our indications for a collinear phase when $\mu_c = 0$ and $\alpha \lesssim 0.8$. Results for the constrained model confirm the presence of the intermediate regime, with a finite negative slope of $n_c(\mu_c)$ in the vicinity of $\mu_c = 0$, separated from a large- μ_c regime where $n_c = 0$ by a succession of discontinuities in the range $1 \leq \mu_c/x_m \leq 2$ (the multiplicity of discontinuities is a finite-size effect). The finite orbital compressibility at and in the vicinity of $\mu_c = 0$, combined with the long-ranged orbital correlations [evidenced e.g. by $S_c(M_a)$ in Fig. 10] constitute similarities between this phase and a bosonic supersolid: in both situations, order develops on one sublattice, while either the number of bosons or the population of c -orbitals can fluctuate on the other sublattices, allowing for a finite compressibility.

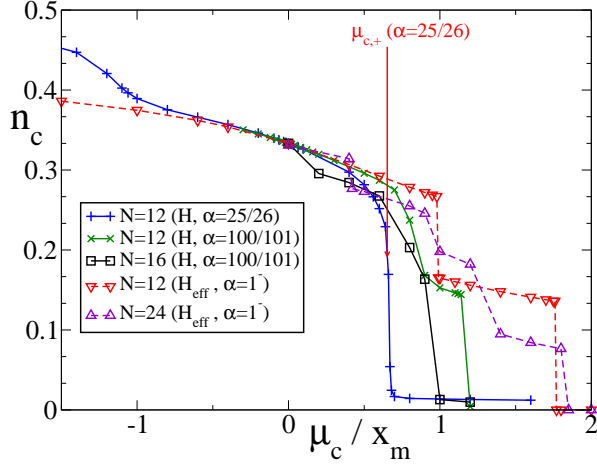


FIG. 13: (Color online) Electron density in c orbitals per site, n_c , as a function of the ratio of μ_c over mixed-exchange amplitude $x_m = \sqrt{(1-\alpha)\alpha}$, either within the full model (\mathcal{H} augmented by the chemical potential term) on periodic clusters ($N = 12, 16$ sites) for different α values; or within the constrained model $H_{\text{eff},c}$ [Eq. (B1)], as obtained for clusters of $N \leq 24$ sites for $\alpha \rightarrow 1$.

- ¹ L. Balents, *Nature (London)* **464**, 199 (2010).
- ² J. van den Brink, *New J. Phys.* **6**, 201 (2004).
- ³ G. Khaliullin and S. Maekawa, *Phys. Rev. Lett.* **85**, 3950 (2000); G. Khaliullin, *Prog. Theor. Phys. Suppl.* **160**, 155 (2005).
- ⁴ H. D. Zhou, Y. J. Jo, J. Fiore Carpinio, G. J. Munoz, C. R. Wiebe, J. G. Cheng, F. Rivadulla, and D. T. Adroja, *Phys. Rev. B* **81**, 212401 (2010).
- ⁵ J. Chaloupka, G. Jackeli, and G. Khaliullin, *Phys. Rev. Lett.* **105**, 027204 (2010); Y. Singh, S. Manni, J. Reuther, T. Berlijn, R. Thomale, W. Ku, S. Trebst, and P. Gegenwart, *ibid.* **108**, 127203 (2012).
- ⁶ K. I. Kugel and D. I. Khomskii, *Sov. Phys. Usp.* **25**, 231 (1982).
- ⁷ V. Fritsch, J. Hemberger, N. Büttgen, E.-W. Scheidt, H.-A. Krug von Nidda, A. Loidl, and V. Tsurkan, *Phys. Rev. Lett.* **92**, 116401 (2004).
- ⁸ F. Vernay, A. Ralko, F. Becca, and F. Mila, *Phys. Rev. B* **74**, 054402 (2006); F. Mila, F. Vernay, A. Ralko, F. Becca, P. Fazekas, and K. Penc, *J. Phys.: Condens. Matter* **19**, 145201 (2007).
- ⁹ A. J. W. Reitsma, L. F. Feiner, and A. M. Oleś, *New J. Phys.* **7**, 121 (2005).
- ¹⁰ B. Normand and A. M. Oleś, *Phys. Rev. B* **78**, 094427 (2008).
- ¹¹ J. Chaloupka and A. M. Oleś, *Phys. Rev. B* **83**, 094406 (2011); A. M. Oleś and J. Chaloupka, *Acta Phys. Polon. A* **121**, 1026 (2012).
- ¹² B. Normand, *Phys. Rev. B* **83**, 064413 (2011).
- ¹³ A. M. Oleś, P. Horsch, L. F. Feiner, and G. Khaliullin, *Phys. Rev. Lett.* **96**, 147205 (2006); A. M. Oleś, *J. Phys.: Condens. Matter* **24**, 313201 (2012).
- ¹⁴ J. van den Brink, P. Horsch, F. Mack, and A. M. Oleś, *Phys. Rev. B* **59**, 6795 (1999).
- ¹⁵ L. Cincio, J. Dziarmaga, and A. M. Oleś, *Phys. Rev. B* **82**, 104416 (2010).
- ¹⁶ Z. Nussinov and G. Ortiz, *Europhys. Lett.* **84**, 36005 (2008); F. Trouselet, A. M. Oleś, and P. Horsch, *ibid.* **91**, 40005 (2010).
- ¹⁷ S. Wenzel and W. Janke, *Phys. Rev. B* **78**, 064402 (2008); S. Wenzel, W. Janke, and A. M. Läuchli, *Phys. Rev. E* **81**, 066702 (2010).
- ¹⁸ Z. Nussinov, M. Biskup, L. Chayes, and J. van den Brink, *Europhys. Lett.* **67**, 990 (2004).
- ¹⁹ A. van Rynbach, S. Todo, and S. Trebst, *Phys. Rev. Lett.* **105**, 146402 (2010).
- ²⁰ J. Oitmaa and C. J. Hamer, *Phys. Rev. B* **83**, 094437 (2011).
- ²¹ S. Wenzel and A. M. Läuchli, *Phys. Rev. Lett.* **106**, 197201 (2011).
- ²² D. S. Rokhsar and S. A. Kivelson, *Phys. Rev. Lett.* **61**, 2376 (1988).
- ²³ This exact degeneracy originates in a symmetry of the model combining a $2\pi/3$ spatial rotation and a permutation of flavor indices; there, the ground states are found in representations with character $e^{i\pm 2\pi/3}$ for this symmetry.
- ²⁴ A. Ralko, M. Mambrini, and D. Poilblanc, *Phys. Rev. B* **80**, 184427 (2009).
- ²⁵ R. Moessner and S. L. Sondhi, *Phys. Rev. Lett.* **86**, 1881 (2001).
- ²⁶ N. Trivedi and D. M. Ceperley, *Phys. Rev. B* **41**, 4552 (1990); M. Calandra Buonauro and S. Sorella, *ibid.* **57**, 11446 (1998).
- ²⁷ A. Ralko, M. Ferrero, F. Becca, D. Ivanov, and F. Mila, *Phys. Rev. B* **71**, 224109 (2005).
- ²⁸ Among maximally flippable states, the non-columnar ones are destabilized at order $p = 3$ or $p = 4$ in perturbation. This is consistent with a scaling $\sim 1/v^3$ for the lowest excitation energies to such states, as found on clusters $N = 36, 48$.
- ²⁹ P. W. Kasteleyn, *Physica* **27**, 1209 (1961).
- ³⁰ For clusters of $N = 8$ sites [within the full model of Eq. (2)] and of $N = 20, 24, 28$ sites [within the effective model of Eq. (15)], which do not possess C_{6v} point group symmetries, $S_c(M_a)$ is

averaged over the ground states of all clusters related to each other by these symmetries.

- ³¹ For the $N = 16$ cluster we also find states, among the lowest excited ones, at momenta $(\pi, 0)$ and $M_a/2$ (and those related by symmetry) with energies comparable to those at high-symmetry points; this is merely a special feature of this cluster, and *not* an indication of any order with 16-site unit cell as one might think: indeed we did not find such a feature for a $N = 32$ cluster which would also accommodate such a phase.
- ³² Y. Chen, P. Zanardi, Z. D. Wang, and F. C. Zhang, *New J. Phys.* **8**, 97 (2006).
- ³³ For the $N = 12$ cluster we computed $\mathcal{S}_{vN}(A)$ on the lowest state

of the representation with $\vec{q} = \Gamma$ and character 1 w.r.t. the rotation-permutation symmetry mentioned in Ref. 23 — this allows to get rid of artefacts of the two-fold ground state degeneracy for $\alpha \leq 0.81(1)$, while the jump observed in Fig. 12(b) around this value reflects well the change of nature of ground state in the TL.

- ³⁴ W. Koshibae and S. Maekawa, *Phys. Rev. Lett.* **91**, 257003 (2003).
- ³⁵ S. R. Hassan, L. de Medici, and A.-M. S. Tremblay, *Phys. Rev. B* **76**, 144420 (2007).
- ³⁶ C. Hotta and N. Furukawa, *Phys. Rev. B* **74**, 193107 (2006).
- ³⁷ S. J. Clarke, A. J. Fowkes, A. Harrison, R. M. Ibberson, and M. J. Rosseinsky, *Chem. Mater.* **10**, 372 (1998).